

# Asphaltenic aggregates are polydisperse oblate cylinders

Keith L. Gawrys<sup>1</sup>, Peter K. Kilpatrick<sup>\*</sup>

*Department of Chemical Engineering, North Carolina State University, Raleigh, NC 27965-7905, USA*

Received 4 November 2004; accepted 6 March 2005

Available online 13 April 2005

## Abstract

Small-angle neutron scattering (SANS) has proven to be very useful for deducing the sizes and morphologies of asphaltenic aggregates in solution. A wide variety of intra-particle structure factors have previously been applied to SANS scattering spectra, but the studies often provided limited information concerning the quality of the fits and the  $Q$  range over which the models were applied. Selection of an appropriate form factor that closely approximates the structure of asphaltenic aggregates is important for determining the properties of asphaltenic aggregates, such as the radius of gyration ( $R_G$ ), molar mass, and apparent fractal dimension. This study evaluates various mono- and polydisperse intra-particle structure factor models as applied to four asphaltene scattering spectra. Agreement of the model fit parameters ( $I_0$  and  $R_G$ ) with those obtained from Guinier analyses suggests that such a form factor model is physically reasonable. Reduced  $\chi^2$  values for each non-linear least squares fit indicates how well a given model fits to the entire  $Q$  range studied for the scattering intensity distribution. In the polydispersity analyses, an analytical function is introduced to model the scattering behavior of oblate cylinders with a Schultz distribution of radii. Results indicate that the polydisperse radius oblate cylinder model best approximates the shape of asphaltenic aggregates.

© 2005 Elsevier Inc. All rights reserved.

*Keywords:* Asphaltenes; Small-angle neutron scattering; Polydispersity

## 1. Introduction

Because of their propensity to aggregate, flocculate, precipitate, and adsorb onto interfaces, the presence of asphaltenes in crude oil poses considerable challenges for the petroleum industry. Asphaltenes are generally defined as the toluene (or benzene) soluble, yet *n*-heptane (or *n*-pentane) insoluble, portion of crude oil. This solubility class definition of asphaltenes suggests a broad distribution of asphaltene molecular structures that vary greatly among crude sources. In general, asphaltenes possess fused ring aromaticity, small aliphatic side chains, and polar heteroatom-containing functional groups (e.g., carboxylic acids, carbonyl, phenol, pyrroles, and pyridines) capable of donating or accepting protons inter- and intra-molecularly [1–5]. Atomic H/C ratios from 1.0 to 1.3 and nitrogen, sulfur, and

oxygen contents of a few weight percent suggest that the asphaltene backbone mostly contains fused aromatic carbon interspersed with occasional polar functional groups [6–8]. The most plausible mechanisms of asphaltene aggregation involve van der Waals dispersion interactions between aromatic rings, hydrogen bonding between polar functional groups, and other charge transfer interactions [9]. Therefore, asphaltene aggregation behavior is likely controlled by the polydispersity, chemical composition, and steric arrangement or inter-connectivity of functional groups in the asphaltene monomers.

Various experimental techniques have previously been applied to study the aggregation behavior of asphaltenes in solution including: near-infrared spectroscopy [10,11], pulsed-field gradient spin echo nuclear magnetic resonance [12,13], vapor pressure osmometry [8,14,15], viscosity measurements [16–19], small-angle X-ray scattering (SAXS) [14,17,20–25], and small-angle neutron scattering (SANS) [8,14,16,21–23,26–39]. Small-angle scattering methods, such as SAXS and SANS, have been useful for deducing the

<sup>\*</sup> Corresponding author. Fax: +1 919 515 3465.

E-mail address: [peter-k@ncsu.edu](mailto:peter-k@ncsu.edu) (P.K. Kilpatrick).

<sup>1</sup> Present address: Nalco Energy Services, Sugar Land, TX 77478, USA.

sizes of asphaltenic aggregates in solution based on assumed particle morphologies. However, a wide variety of intra-particle structure factors have previously been applied to the SAXS and SANS scattering spectra of asphaltene solutions, often with limited information concerning the quality of the fits and the data range over which the models were applied. The monodisperse and polydisperse form factors typically applied to asphaltenic aggregates include spheres, cylinders (oblate and prolate), and ellipsoids (oblate and prolate). It is unlikely that every model accurately describes the structure of asphaltenic aggregates.

This study compares various intra-particle structure factor models applied to scattering intensity curves obtained from solutions of Hondo, Canadon Seco, and Arab Heavy asphaltenes at different solvent conditions (i.e., a dispersive solvent and a flocculating solvent). A set of criteria is established to assess the quality of the data fits. The values of the non-linear least-squares fit parameters ( $I_0$  and  $R_G$ ) are compared to those obtained from the Guinier approximation to determine if the parameters obtained are molecularly reasonable. Furthermore, the reduced  $\chi^2$  values from each model fit are directly compared to assess the quality of each model with respect to other models. An analytical function is derived in the analyses to model the scattering behavior of polydisperse oblate cylinders with a Schultz distribution of radii. Once a model is determined to accurately describe the structure of asphaltenic aggregates, additional parameters may be calculated from the scattering data, including aggregate molar masses, second virial coefficients, and percentage of solvent entrainment within aggregates [40,41].

## 2. Materials and methods

Asphaltenes were precipitated from their corresponding source crude oils by the addition of excess *n*-heptane (40:1 v/v) using the procedure of Spiecker et al. [8]. Asphaltenes isolated from Canadon Seco and Arab Heavy asphaltenes were dried without further washing. The Hondo asphaltenes precipitated by the above procedure were washed with *n*-heptane via Soxhlet extraction to remove any co-precipitated maltenes. A second Soxhlet extraction was performed using toluene as the wash solvent to dissolve the asphaltenes from the filter paper, leaving behind any inorganic insolubles. Both extraction procedures continued until the overflow from the extractions became colorless. Most of the solvent was removed from the asphaltene solutions by rotary evaporation under partial vacuum at 60 °C. Once nearly dry, the asphaltenes were moved into a nitrogen-flushed vacuum oven at 50 °C for 24 h. The dry asphaltenes were transferred to glass jars and stored under argon to prevent oxidation. The isolated asphaltenes were characterized by combustion elemental analysis at the University of Alberta (Department of Chemistry, Edmonton, AB, Canada) using a Carlo Erba instrument. Elemental analysis results for the isolated asphaltenes are presented in Table 1. Hondo asphaltenes were

Table 1  
Elemental composition (wt%) of asphaltene samples

Asphaltene	C	H	N	S	O	H/C (atomic)
Hondo	80.72	8.27	1.96	6.87	2.18	1.29
Canadon Seco	88.21	8.22	1.32	0.52	1.73	1.11
Arab Heavy	81.25	7.77	1.02	8.32	1.64	1.14

less aromatic with higher polar heteroatom content than the corresponding Canadon Seco and Arab Heavy asphaltenes.

Two solutions with mass concentration of 1% (w/w) were prepared by dissolving the Hondo asphaltenes in mixtures of 90:10 *d*-toluene:*d*-methanol (v/v) and 40:60 *d*-heptane:*d*-toluene (v/v). Two additional solutions with mass concentration of 1% (w/w) were prepared by dissolving Canadon Seco and Arab Heavy asphaltenes in *d*-toluene. Solvents were obtained from CDN Isotopes and had >99.9% chemical purity and >99.5% perdeuteration. During the sample preparation, *d*-toluene was initially added to the dry asphaltenes and the solution was subjected to constant, gentle shaking until the asphaltenes were completely dissolved. Upon dissolution of the asphaltenes, the second solvent (i.e., *d*-methanol or *d*-heptane) was added to the solutions. The solutions were allowed to equilibrate for at least one week prior to performing the scattering experiments.

SANS measurements were performed on the small-angle neutron diffractometer (SAND) at the Intense Pulsed Neutron Source (IPNS) Division of Argonne National Laboratory (Argonne, IL). The sample-to-detector distance was fixed at 2 m. Neutrons were collected on an area detector (40 × 40 cm, 4 to 6 mm FWHM resolution). The instrument geometry and neutron wavelength values bound the operating  $Q$  range according to

$$Q = \frac{4\pi}{\lambda} \sin \theta, \quad (1)$$

where  $\theta$  is half the scattering angle and  $\lambda$  is the neutron wavelength. The available  $Q$  range for the SAND instrument extended from 0.0035 to 2 Å<sup>-1</sup> and was adequate to yield scattering curves that cover the full  $Q$  range for asphaltenic aggregates. Spectra were collected at 25 °C in cylindrical quartz sample cells (NGS Precision) with a path length of 2 mm. A typical scattering experiment consisted of 15 min of detecting neutron transmission through the samples followed by 60 min of scattering. The absolute scattering intensity distribution,  $I(Q)$ , for each sample was obtained from the total detector counts corrected for background radiation, neutron transmission through the sample, scattering from the quartz cell, and detector sensitivity. Scattering intensity versus scattering angle ( $I(Q)$  vs  $Q$ ) curves were fit to various intra-particle structure factor models using the macro functions authored by Kenneth Littrell and provided by Argonne National Laboratory for use with IgorPro software. The fitting function for polydisperse radius oblate cylinders was written by the authors.

### 3. Model fitting

A variety of models can be applied to the scattering intensity distribution,  $I(Q)$ , of an asphaltene solution in order to obtain information concerning the morphology of the scattered particle. For example, the Guinier approximation [42] provides a means of estimating aggregate sizes without specifying the particle geometry as given by

$$I(Q) = I_0 \exp(-Q^2 R_G^2/3), \quad (2)$$

where  $I_0$  is the scattering intensity extrapolated to  $Q = 0$ .  $R_G$  is the radius of gyration defined as the root mean squared distance of all atoms from the center of mass of the particle. The zero- $Q$  scattering intensity,  $I_0$ , provides additional information concerning the particle geometry and is related to the weight-averaged molecular weight of the aggregates.

Another scattering function that describes the behavior of aggregates without specifying the particle geometry is the small-particle mass-fractal model [43] given by

$$I(Q) = I_0 \frac{\sin[(D-1) \tan^{-1}(Q\xi)]}{(D-1)Q\xi(1+Q^2\xi^2)^{(D-1)/2}}, \quad (3)$$

where  $D$  and  $\xi$  are the fractal dimension and exponential cut-off length for fractal aggregation, respectively. Mass fractals are defined by the scaling relationship between the total particle mass contained within a given radius,  $r$ , according to  $M \sim r^D$ . Equation (3) is a simplification of the mass-fractal model introduced by Chen and Teixeira [44] that describes the aggregates as a three-dimensional agglomeration consisting of elementary spherical particles with radius,  $R$ , and having a fractal-like nature. The small-particle mass-fractal assumes that scattering from the elementary spherical particles is negligible (i.e.,  $\xi \gg R$  and  $Q_{\max} R \ll 1$ ).

Alternatives to the Guinier and mass fractal analyses are those based on form factors. With a monodisperse system, the scattering intensity distribution is proportional to the product of an intra-particle structure factor,  $P(Q)$ , and an inter-particle structure factor,  $S(Q)$ , as given by

$$I(Q) = I_0 P(Q) S(Q) = I_0 |F(Q)|^2 S(Q). \quad (4)$$

In the limit of low particle density, the solution becomes ideal and the inter-particle structure factor is assumed unity. All of the models presented in this study neglect interactions between particles. In the above equation,  $|F(Q)|$  is the amplitude of the particle form factor defined by

$$|F(Q)| = \int [\rho_p(r) - \rho_s] \exp(iQ \cdot r) dr, \quad (5)$$

where  $\rho_p(r)$  is the particle scattering length density at distance  $r$  from the particle and  $\rho_s$  is the solvent scattering length density. The particle form factor is geometry dependent. Since particles are assumed to be randomly oriented, anisotropic particles must be averaged over spatial orientation. An extensive review of form factor models for various monodisperse particle shapes is provided by Pedersen [45].

The scattering intensity distribution for a polydisperse system is proportional to the ensemble average of the intra-particle structure factor (i.e., assuming no inter-particle interactions) as given by

$$I(Q) = \int_0^\infty I_0 P(Q, x) f(x) dx, \quad (6)$$

where  $f(x)$  is a normalized distribution function for size parameter,  $x$ . Examples of size-distribution functions used to describe polydispersity in asphaltene aggregate sizes include the log-normal distribution [14,23] and the Schultz distribution [29]. The general formula for a log-normal distribution is given by

$$f_{\ln}(x) = \frac{1}{\sqrt{2\pi}\sigma x} \exp\left(-\frac{1}{2} \left[\frac{\ln(x) - \ln(x_{\text{avg}})}{\sigma}\right]^2\right), \quad (7)$$

where  $\sigma$  and  $x_{\text{avg}}$  are the standard deviation and average size parameter value of the log-normal distribution, respectively. The general formula for a Schultz distribution is given by

$$f_s(x) = \frac{x^z}{\Gamma(z+1)} \left[\frac{z+1}{x_{\text{avg}}}\right]^{z+1} \exp\left(-\frac{(z+1)x}{x_{\text{avg}}}\right), \quad (8)$$

where  $\Gamma(n)$  is the gamma function and  $z$  is the polydispersity parameter defined by

$$z = \left(\frac{x_{\text{avg}}}{\sigma}\right)^2 - 1. \quad (9)$$

Both of the distribution functions are right-hand skewed, indicating the scattering intensity distributions are weighted more heavily by contributions from larger scatterers in solution. The polydisperse form factors presented in this study assume a Schultz distribution of particle sizes (e.g., polydisperse spheres and polydisperse length cylinders) that allows for direct analytical solutions to the integral in Eq. (6).

The various intra-particle structure factors applied to the SANS scattering intensity curves for asphaltene solutions in this study include monodisperse spheres, monodisperse oblate cylinders, monodisperse prolate cylinders, polydisperse spheres, polydisperse length oblate cylinders, and polydisperse radius oblate cylinders. The intra-particle structure factor for a homogeneous sphere with radius  $R$  is given by

$$P_{\text{sphere}}(Q) = \left(\frac{3[\sin(QR) - QR \cos(QR)]}{(QR)^3}\right)^2. \quad (10)$$

Kotlarchyk and Chen [46] derived an analytical expression for a polydisperse intra-particle structure factor with a Schultz distribution of radii by combining Eqs. (6), (8) and (10). Sheu extended the analyses of polydisperse spheres to several other distribution functions [47] and justified the use of the Schultz spherical model for asphaltene solutions in toluene [29].

The intra-particle structure factor for a monodisperse cylinder (oblate or prolate) with radius  $R$  and length  $L$  is

given by

$$P_{\text{cyl}}(Q) = \int_{\beta=0}^{\pi/2} \left[ \frac{2J_1(QR \sin \beta)}{QR \sin \beta} \frac{\sin((QL \cos \beta)/2)}{(QL \cos \beta)/2} \right]^2 \times \sin \beta \, d\beta, \quad (11)$$

where  $J_1(x)$  represents a first-order Bessel function of the first kind and  $\beta$  is the orientational averaging angle. One simplification of Eq. (11) for a monodisperse flat disk (i.e., oblate cylinder) may be written as [48]

$$P_{\text{ob},1}(Q) = 2 \left[ \frac{\sin(QL/2)}{QL/2} \right]^2 \left[ \frac{1 - J_1(2QR)/QR}{(QR)^2} \right]. \quad (12)$$

Alternatively, the high  $Q$  region of a monodisperse flat disk may also be described by an exponential approximation [42] given by

$$P_{\text{ob},2}(Q) = \frac{2}{(QR)^2} \exp\left(-\frac{(QL)^2}{12}\right). \quad (13)$$

Sheu [47] derived an explicit form of the intra-particle structure factor for a cylinder with a Schultz distribution of particle lengths by combining Eqs. (6), (8), and (11). Similar attempts to model the intra-particle structure factor for a cylinder with a Schultz distribution of radii require numerical integration techniques (e.g., Gaussian quadrature) to solve the ensemble average integral in Eq. (6). A direct analytical solution for the case of polydisperse oblate cylinders with a Schultz distribution of radii is obtained by taking advantage of the flat disk approximations given in Eqs. (12) and (13). Specific details concerning the model development are found in Appendix A.

#### 4. Results and discussion

Scattering intensity versus scattering angle ( $I(Q)$  vs  $Q$ ) curves of 1% (w/w) solutions of Hondo asphaltenes in 90:10  $d$ -toluene: $d$ -methanol (v/v) and 40:60  $d$ -heptane: $d$ -toluene (v/v) are shown in Fig. 1. The sharp rise in the scattering intensity at low  $Q$  values for Hondo asphaltenes in 40:60  $d$ -heptane: $d$ -toluene ( $\Delta$ ) indicated the presence of micron sized flocs in solution. A small percentage of Hondo asphaltenes are precipitated at this concentration of heptane and toluene [8]. Similar Porod-like power law behavior was observed for asphaltene solutions and crude oil blends [34, 38]. For example, Roux et al. [34] observed a low  $Q$  feature for Safaniya asphaltenes in toluene at 8 and 20 °C that diminished in intensity with heating. This observation suggests that an increase in solution temperature is effective in dissolving these flocs. It is not possible to determine the size of the flocs from these scattering experiments, because the Porod-like upturns do not exhibit a plateau behavior at the lowest scattering angles. The three lowest  $Q$  data points for this solution were fit to a power law function with an exponent of  $-4$  (i.e.,  $I(Q) \sim Q^{-4}$ ). The corresponding power law fit appears as the dashed line in Fig. 1. This power law function was subtracted from the original scattering data over the entire available  $Q$  range. As seen in the figure, the resulting power law subtracted scattering curve ( $\circ$ ) reveals the full  $Q$  range of the scattering behavior from nanoscale aggregates in this solution. The various model fits were applied to this modified scattering curve in order to study the morphology of the nanoscale aggregates. A similar power law correction was applied to the scattering intensity distribution for Canadon Seco asphaltenes in  $d$ -toluene. The scattering intensity curves for Hondo asphaltenes in

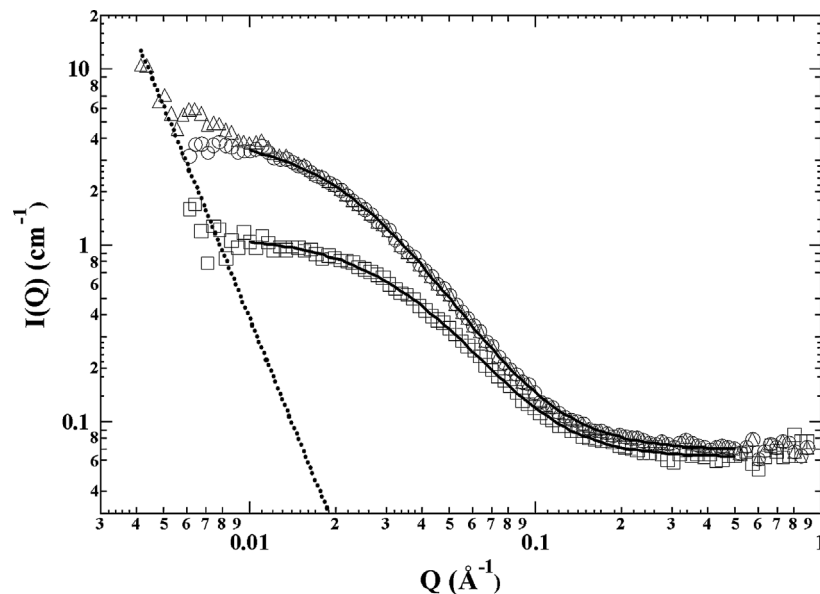


Fig. 1. Low  $Q$  power law correction and small-particle mass-fractal fits to Hondo asphaltenes in mixed solvents. ( $\Delta$ ) Hondo asphaltenes in 40:60  $d$ -heptane: $d$ -toluene; ( $\cdots$ ) low  $Q$  power law fit to 40:60  $d$ -heptane: $d$ -toluene; ( $\circ$ ) power law subtracted data for 40:60  $d$ -heptane: $d$ -toluene; ( $\square$ ) Hondo asphaltenes in 90:10  $d$ -toluene: $d$ -methanol; ( $—$ ) small-particle mass-fractal fits with constant background.

Table 2  
Comparison of fit parameters obtained from the Guinier approximation and small-particle mass-fractal models

Asphaltene	Guinier approximation			Small-particle mass-fractal				
	$I_0$ (cm <sup>-1</sup> )	$R_G$ (Å)	$QR_G$	$I_0$ (cm <sup>-1</sup> )	$\xi$ (Å)	$D$	$R_G$ (Å)	$\chi^2$
Hondo (90:10 Tol:MeOD)	1.08 ± 0.03	43 ± 3	0.986	1.07 ± 0.02	23.9 ± 0.5	2.61 ± 0.02	52 ± 2	0.8091
Hondo (40:60 H:T)	4.2 ± 0.2	71 ± 5	1.005	4.15 ± 0.06	38.7 ± 0.6	2.52 ± 0.02	82 ± 2	1.6089
Canadon Seco (toluene)	3.0 ± 0.1	58 ± 5	0.945	3.20 ± 0.05	34.3 ± 0.6	2.63 ± 0.02	75 ± 2	1.7325
Arab Heavy (toluene)	1.48 ± 0.04	45 ± 3	0.990	1.49 ± 0.02	22.0 ± 0.5	2.76 ± 0.03	50 ± 2	0.9080

90:10 *d*-toluene:*d*-methanol and Arab Heavy asphaltenes in *d*-toluene did not possess significant low  $Q$  features, indicating that the asphaltenic aggregates were completely soluble in these solvents and, hence, no power law corrections were needed for these samples prior to performing the model fits.

Initial estimates of the nanoparticle  $I_0$  and  $R_G$  parameters were obtained by applying the Guinier approximation (Eq. (2)) to the modified scattering curves (see Table 2). As expected, larger  $I_0$  and  $R_G$  values were observed for Hondo asphaltenes as the solvent quality decreased to 40:60 *d*-heptane:*d*-toluene. It should be noted that the fits to the Guinier approximation were limited to 10–17 total data points and represented only the lowest  $Q$  region of the scattering spectra. Additional estimates of the aggregate size are obtained from general models, such as the small-particle mass-fractal model, that fit the full range of  $Q$  values in the scattering spectra.

Fits of the small-particle mass-fractal model to the scattering intensity curves for both solutions of Hondo asphaltenes are shown as the solid lines in Fig. 1. The  $Q$  range over which the small-particle mass fractal and subsequent model fits were applied was fixed between 0.01 and 0.52 Å<sup>-1</sup>. A constant background term was included in the model fits to account for incoherent scattering from all nuclei with non-zero spin in the solvent and solute. The values of the incoherent background terms obtained from the small-particle mass-fractal fits were also fixed during the subsequent fits of the remaining intra-particle structure factors. The values of the fit parameters obtained from the small-particle mass-fractal model are shown in Table 2. The radius of gyration was determined from the model fit parameters by

$$R_G^2 = D(D + 1)\xi^2/2. \quad (14)$$

As indicated in the table, the  $I_0$  values obtained from the mass-fractal model fits generally agreed with those obtained from the Guinier approximation within 12%; however, the  $R_G$  values obtained from the mass-fractal fits generally over-predicted the corresponding Guinier values by approximately 20 to 30%. The  $\chi_{\text{red}}^2$  parameter in Table 2 describes the quality of the model fit reduced by the number of degrees of freedom ( $n - 1$ ) and is defined by

$$\chi_{\text{red}}^2 = \sum_{k=1}^n \left( \frac{I_k - I_{k,\text{calculated}}}{\delta I_k} \right)^2 / (n - 1), \quad (15)$$

where  $I_k$ ,  $\delta I_k$ , and  $I_{k,\text{calculated}}$  are the experimentally observed scattering intensity, experimental uncertainty in the

scattering intensity, and the calculated scattering intensity for data point  $k$ , respectively. In practical applications, values of the reduced  $\chi^2$  that approach unity suggest that the given model fits well to the experimental data.

The near-unity values of the reduced  $\chi^2$  for the mass-fractal fits suggest that the small-particle mass-fractal model may be effectively used to model the aggregation behavior of asphaltenic aggregates in solution. However, relating the model to a physical description of the appearance of asphaltenic aggregates in solution is more difficult. For example, questions arise concerning the nature of the small-particles that compose the mass-fractal asphaltene aggregate. Ras-samdana and Sahimi [49] estimated that the mass-to-particle size scaling relationship for diffusion limited cluster–cluster aggregates with a nanoparticle fractal dimension of 2.5 is consistent with a primary particle size of ~5.8 Å. This prediction is supported by small-angle X-ray scattering [20] and gel permeation chromatography [50] data that modeled the molecular structure of asphaltenes as thin disks with approximate thickness of 4 Å. X-ray diffraction experiments on Ratawi and Kuwaiti asphaltenes [51] suggested an average layer diameter of aromatic sheets between 7 and 10 Å, and an average distance between aromatic sheets between 3.5 and 3.7 Å. Considering these observations, the elementary particles constituting an asphaltene mass-fractal aggregate might consist of stacks of one to two aromatic sheets, possibly connected to similar aromatic moieties by short, aliphatic linkages. For example, a schematic representation of a possible asphaltene monomer and an asphaltenic aggregate consisting of four monomers is presented in Fig. 2.

The values of the  $I_0$  and  $R_G$  parameters obtained from the Guinier fits, as well as the quality of fit (reduced  $\chi^2$ ) parameter from the various intra-particle structure factor fits, were used as a basis for assessing the particle geometry that best describes the geometric morphology of asphaltenic aggregates in solution. Example fits of monodisperse sphere, prolate cylinder, and oblate cylinder intra-particle structure factors to Hondo asphaltenes in 90:10 *d*-toluene:*d*-methanol are presented in Fig. 3. The values of the fit parameters for each of the models are shown in Table 3. The radius of gyration for a solid sphere is obtained from the value of the radius parameter as given by

$$R_G^2 = \frac{3}{5} R^2. \quad (16)$$

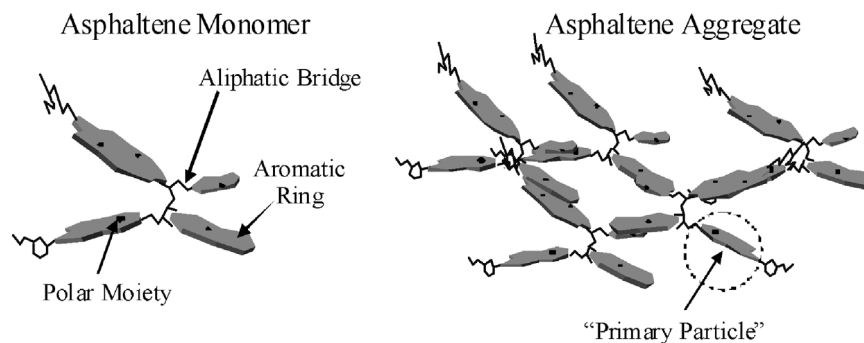


Fig. 2. Schematic representation of an asphaltene monomer and an asphaltene aggregate consisting of four monomers.

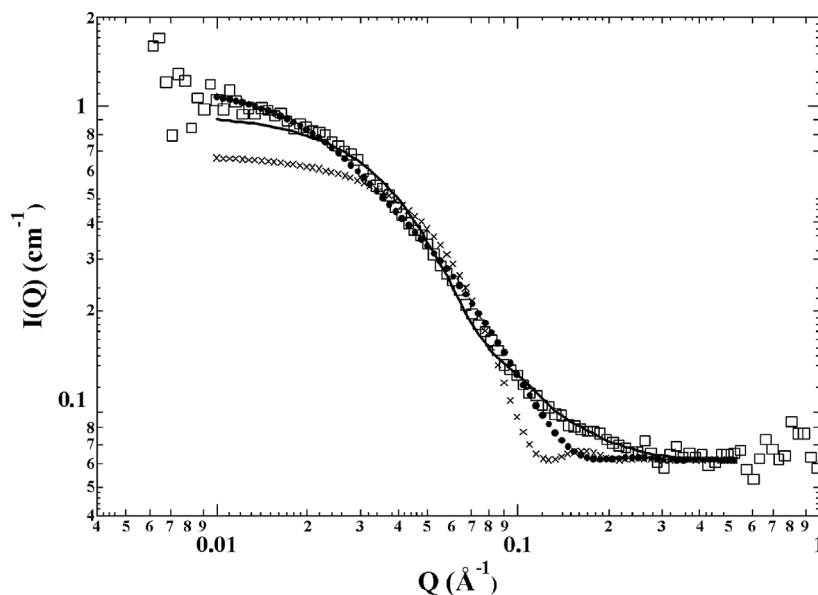


Fig. 3. Fits of monodisperse sphere (×), monodisperse prolate cylinder (●), and monodisperse oblate cylinder (—) models to Hondo asphaltenes (□) in 90:10 *d*-toluene:*d*-methanol.

The radius of gyration for a circular cylinder is given by

$$R_G^2 = \frac{L^2}{12} + \frac{R^2}{2}. \quad (17)$$

As indicated in the table, the monodisperse sphere fits had the poorest fit quality and were observed to under-predict the values of the  $I_0$  and  $R_G$  fit parameters obtained from the Guinier fits. The monodisperse prolate cylinder fit provided molecularly reasonable size parameters for Hondo asphaltenes in 90:10 *d*-toluene:*d*-methanol and Arab Heavy asphaltenes in *d*-toluene, but not for the more intensely scattering Hondo asphaltenes in 40:60 *d*-heptane:*d*-toluene or the Canadon Seco asphaltenes in *d*-toluene. In fact, the  $I_0$  and  $L_{\text{avg}}$  values for these two solutions of asphaltenes were excessively large, suggesting the prolate cylinder model does not accurately describe the asphaltene aggregate shape. The oblate cylinder model provided better agreement for the more intensely scattering samples to the Guinier parameters than the other monodisperse models. Likewise, the values of the reduced  $\chi^2$  parameter were minimized for the

oblate cylinder model fits compared to other molecularly reasonable monodisperse fits. These results indicate that the morphologies of asphaltene aggregates are likely similar to those of flat disks; however, the chemical polydispersity of asphaltenes suggests that the particle sizes of asphaltene aggregates are likely polydisperse as well. The reduced  $\chi^2$  values for the Schultz polydisperse spheres show an improvement in fit quality over the monodisperse sphere model; however, the reduced  $\chi^2$  values are still larger than those for the monodisperse oblate cylinder fits. In addition, the average  $R_G$  values obtained from the polydisperse sphere fits were excessively small and not molecularly reasonable. Since the oblate cylinder fits provided the lowest reduced  $\chi^2$  values of the various monodisperse models, attempts were made to introduce Schultz distributions of particle lengths and radii for the oblate cylinder model.

Fig. 4 presents reduced  $\chi^2$  values for fits of polydisperse length (○) and polydisperse radius (□) oblate cylinders at fixed values of the polydispersity parameter for Hondo asphaltenes in 90:10 *d*-toluene:*d*-methanol. In this case, the

Table 3  
Comparison of fit parameters obtained from various monodisperse and polydisperse form factor models

Model fit	$I_0$ (cm <sup>-1</sup> )	$R_{\text{avg}}$ (Å)	$\sigma_R$ (Å)	$L_{\text{avg}}$ (Å)	$\sigma_L$ (Å)	$\langle R_G^2 \rangle^{1/2}$ (Å)	$\chi^2$
Hondo asphaltenes (90:10 toluene:methanol)							
Monodisperse spheres	0.62 ± 0.01	35.7 ± 0.1	–	–	–	27.7 ± 0.1	48.381
Monodisperse prolate cylinders	1.12 ± 0.02	20.7 ± 0.1	–	186 ± 5	–	56 ± 2	9.5199
Monodisperse oblate cylinders	0.88 ± 0.01	52.8 ± 0.3	–	12.2 ± 0.6	–	38 ± 2	4.3489
Schultz polyradius spheres	0.91 ± 0.01	0.69 ± 0.02	2.40 ± 0.04	–	–	0.68 ± 0.02	4.9721
Schultz polylength oblate cylinders	0.88 ± 0.01	52.7 ± 0.3	–	12.1 ± 0.6	0.5	38 ± 2	4.3488
Schultz polyradius oblate cylinders	0.98 ± 0.01	42.6 ± 0.9	13.5 ± 0.3	15.1 ± 0.6	–	45 ± 4	1.3845
Hondo asphaltenes (40:60 heptane:toluene)							
Monodisperse spheres	1.61 ± 0.01	44.1 ± 0.1	–	–	–	34.2 ± 0.1	173.7
Monodisperse prolate cylinders	179 ± 1	7.6 ± 0.2	–	11280 ± 50	–	3260 ± 30	9.5825
Monodisperse oblate cylinders	3.29 ± 0.03	79.6 ± 0.4	–	20.3 ± 0.3	–	57 ± 1	12.833
Schultz polyradius spheres	2.92 ± 0.02	0.55 ± 0.04	2.52 ± 0.08	–	–	0.43 ± 0.03	26.086
Schultz polylength oblate cylinders	3.29 ± 0.03	79.5 ± 0.4	–	19.9 ± 0.3	2	83 ± 2	12.830
Schultz polyradius oblate cylinders	4.14 ± 0.04	69.4 ± 0.7	22.3 ± 0.1	20.5 ± 0.3	–	73 ± 2	5.7508
Canadon Seco asphaltenes (toluene)							
Monodisperse spheres	1.43 ± 0.01	44.8 ± 0.1	–	–	–	34.7 ± 0.1	125.98
Monodisperse prolate cylinders	151 ± 1	8.4 ± 0.3	–	11260 ± 60	–	3300 ± 100	8.1415
Monodisperse oblate cylinders	2.56 ± 0.02	75.3 ± 0.4	–	20.5 ± 0.4	–	54 ± 1	11.548
Schultz polyradius spheres	2.48 ± 0.02	0.66 ± 0.05	2.8 ± 0.1	–	–	0.51 ± 0.04	13.895
Schultz polylength oblate cylinders	2.55 ± 0.02	74.7 ± 0.4	–	13.7 ± 0.8	7	53 ± 3	11.254
Schultz polyradius oblate cylinders	2.84 ± 0.03	60 ± 1	18.9 ± 0.3	25.6 ± 0.4	–	58 ± 5	2.9527
Arab Heavy asphaltenes (toluene)							
Monodisperse spheres	0.88 ± 0.01	35.6 ± 0.1	–	–	–	27.6 ± 0.1	73.381
Monodisperse prolate cylinders	1.66 ± 0.03	21.2 ± 0.1	–	194 ± 5	–	58 ± 2	12.303
Monodisperse oblate cylinders	1.26 ± 0.01	52.6 ± 0.3	–	17.1 ± 0.4	–	38 ± 1	6.5966
Schultz polyradius spheres	1.33 ± 0.01	0.71 ± 0.04	2.47 ± 0.07	–	–	0.55 ± 0.03	4.2643
Schultz polylength oblate cylinders	1.26 ± 0.01	52.5 ± 0.3	–	16.6 ± 0.4	2	83 ± 2	6.5948
Schultz polyradius oblate cylinders	1.38 ± 0.01	41.4 ± 0.9	13.2 ± 0.2	20.8 ± 0.7	–	45 ± 3	1.8979

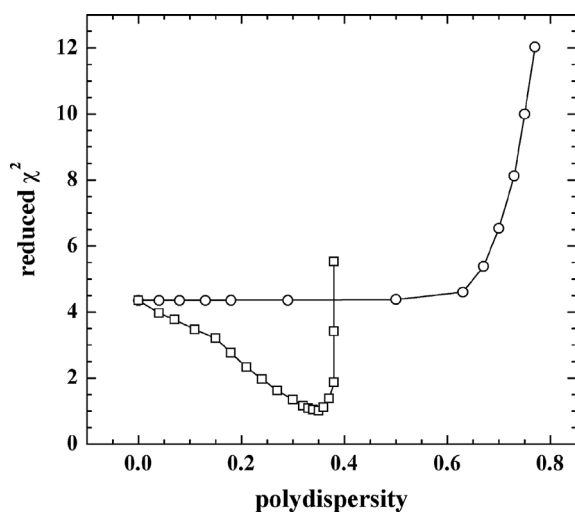


Fig. 4. Reduced  $\chi^2$  values at various polydispersity parameters for fits of (○) polydisperse length oblate cylindrical and (□) polydisperse radius oblate cylindrical models to Hondo asphaltenes in 90:10 *d*-toluene: *d*-methanol.

polydispersity parameter,  $p$ , is defined by

$$p = \frac{\sigma_x}{x_{\text{avg}}}, \quad (18)$$

where  $\sigma_x$  and  $x_{\text{avg}}$  are the standard deviation and average size parameter values of the Schultz distribution, respec-

tively. The value of the reduced  $\chi^2$  for the fit at polydispersity of zero represents the least-squares fit to a monodisperse oblate cylinder model. Fig. 4 suggests that the incorporation of length polydispersity at fixed particle radius does not significantly improve the quality of the fit. For the case presented, the monodisperse oblate cylinder model fit the scattering intensity distribution better than the Schultz polydisperse length oblate cylinder model, regardless of the assumed polydispersity parameter. On the other hand, significant improvement in the quality of the model fits was observed when a Schultz distribution of particle radii was assumed for the aggregates at fixed particle length. As indicated in Fig. 4, the value of the reduced  $\chi^2$  parameter was observed to decrease with increasing radius polydispersity with a minimum in the reduced  $\chi^2$  at a polydispersity value of 0.35. The quality of the model fits declined rapidly at values above the optimum polydispersity value. These results agree with the previous results of Herzog et al. [20] and Bardon et al. [14] that suggest the structure of asphaltenic aggregates may be represented using a distribution of thin disks of fixed thickness and polydisperse radii.

The optimum values of  $I_0$ , the average radius, length, and radius spread for the two solutions of Hondo asphaltenes were determined by non-linear least-squares fitting of the scattering intensity curves to the Schultz polydisperse radius oblate cylinder model as shown in Fig. 5. Unlike Fig. 4, the

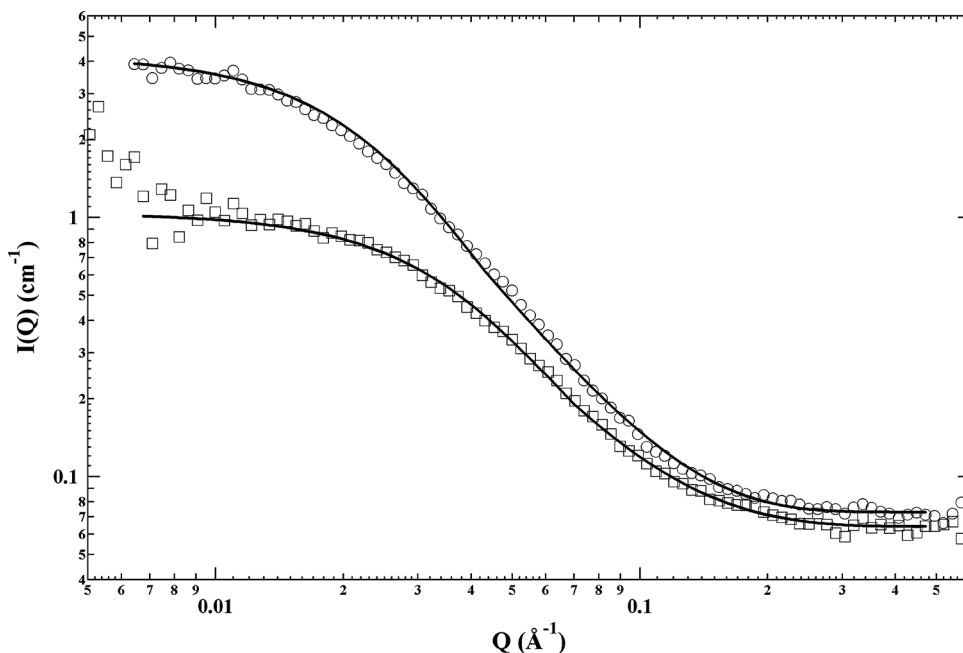


Fig. 5. Fits of a polydisperse radius oblate cylinder form factor to Hondo asphaltenes in (○) 40:60 *d*-heptane:*d*-toluene and (□) 90:10 *d*-toluene:*d*-methanol. Solid lines represent the model fits.

constraint on the polydispersity parameter was relaxed for these fits. The values of the fit parameters obtained from the fits of the scattering spectra to the polydisperse radius oblate cylinder model are shown in Table 3. The radius of gyration for a system of polydisperse radius cylinders is given by [32]

$$\langle R_G \rangle^2 = \frac{L^2}{3} + \frac{R_{\text{avg}}^2}{2} \frac{(z+6)(z+5)}{(z+1)^2}. \quad (19)$$

As indicated in Tables 2 and 3, the fit quality of the Schultz polydisperse radius oblate cylinder model was consistently better than that of the other geometric form factor models. Furthermore, the values of the  $I_0$  and average  $R_G$  parameters for the polyradius cylinder agreed with the parameters obtained from the Guinier fits within statistical uncertainty. Such agreement in the fit parameters was not observed with similar consistency for the other intra-particle structure factor models.

## 5. Conclusions

Various intra-particle structure factor models have been applied in the past to determine aggregate size and  $I_0$  parameters from scattering intensity curves of asphaltene solutions, but not all of these models accurately reflected the morphology of the asphaltenic aggregates in solution. Here we applied several intra-particle structure factor models to the scattering intensity curves for solutions of asphaltenes in three different solvents. The reduced  $\chi^2$  values from the fits were used as a criterion to assess the quality of fit. Comparison of  $I_0$  and  $R_G$  values obtained from the fits to those

obtained from Guinier analyses suggested that the obtained fit parameters were physically reasonable.

The fits of scattering intensity curves to the monodisperse models were useful in determining the general shape of the asphaltenic aggregates; however, it is well known that asphaltene molecules are polydisperse and one would expect the aggregates formed from the interactions of individual molecules to be polydisperse as well. In the cases studied, the monodisperse oblate cylinder model provided a better quality of fit and/or better agreement with the Guinier parameters than the other monodisperse models. When length and radius polydispersity was introduced to the oblate cylinder fits, only the inclusion of radius polydispersity was observed to significantly improve the fit quality over the monodisperse case. The inclusion of polydispersity tended to complicate the analyses of scattering intensity curves as an additional integral is introduced to calculate to ensemble average of the polydisperse size parameter within a distribution function. In many cases, the ensemble average integral must be solved using numerical techniques, such as Gaussian quadrature. The inclusion of numerical integration techniques often significantly increases the computing time for the non-linear least-squares regression. In this study, a direct analytical function was derived for the scattering of polydisperse radius oblate cylinders using approximations for the form factor of a flat disk, as well as a polynomial expansion of the first-order Bessel function of the first kind. The new function fit well to the scattering intensity curves studied, both in terms of overall fit quality (i.e., reduced  $\chi^2$ ) and comparison to the Guinier parameters (i.e.,  $I_0$  and  $R_G$ ). The observations that the parameters obtained from the polydisperse radius oblate cylinder and Guinier fits agreed

within experimental uncertainty and that the reduced  $\chi^2$  values for the polydisperse cylinder fits were consistently lower than those of other geometric form factors, regardless of the solute chemistry or solvent quality, suggests that the asphaltene aggregate structure is best described by a polydisperse flat disk (or polydisperse flat ellipsoid) model. The selection of an appropriate model for the macrostructure of asphaltenic aggregates is important for the calculation of additional parameters from the scattering data, such as the aggregate molecular weight, second virial coefficients, and percentage of solvent entrainment within asphaltenic aggregates.

## Acknowledgments

This research is supported by the Petroleum Environmental Research Forum, ExxonMobil, Shell, Equilon, Chevron-Texaco, Nalco Energy Services Division, Champion Technologies, National Science Foundation Grants (CTS981727), and the NSF Graduate Research Fellowship Program. This work benefited from the use of facilities in the Intense Pulsed Neutron Source and the Chemistry Division, which is funded by the U.S. Department of Energy, Office of Basic Energy Sciences under contract W-31-109-ENG-38 to the University of Chicago. We would particularly like to thank Pappannan Thiyagarajan and Denis Wozniak of the Intense Pulsed Neutron Source Division at Argonne National Laboratory for their assistance with the SAND instrument. We would also like to thank Matthew B. Smith, M. Lupe Marques, George Blankenship, and Vincent Verruto for helping with the sample preparation and SANS data collection.

## Appendix A

The scattering intensity distribution for a system with radius polydispersity is proportional to the normalized average of the intra-particle structure factor (i.e., neglecting inter-particle interactions) as given by [47]

$$I(Q) = \frac{\phi(\Delta\rho)^2 \langle V^2 \rangle}{\langle V \rangle} \langle P(Q) \rangle = I_0 \langle P(Q) \rangle, \quad (\text{A.1})$$

where  $\phi$  is the volume fraction of scatterers,  $\Delta\rho$  is the scattering length density difference between the solvent and solute,  $\langle V \rangle$  is the first moment of the particle volume, and  $\langle V^2 \rangle$  is the second moment of the particle volume. The normalized average of the intra-particle structure factor is given by

$$\langle P(Q) \rangle = \frac{\int_0^\infty P(Q, R) V^2 f(R) dR}{\int_0^\infty V^2 f(R) dR}, \quad (\text{A.2})$$

where  $f(R)$  is a normalized distribution function for the radius parameter,  $R$ . In the case presented, a Schultz distribution of radii is assumed,

$$f_s(R) = \frac{R^z}{\Gamma(z+1)} \left[ \frac{z+1}{R_{\text{avg}}} \right]^{z+1} \exp\left(-\frac{(z+1)R}{R_{\text{avg}}}\right), \quad (\text{A.3})$$

where  $\Gamma(n)$  is the gamma function,  $R_{\text{avg}}$  is the average particle radius, and  $z$  is the polydispersity parameter defined by

$$z = \left( \frac{R_{\text{avg}}}{\sigma} \right)^2 - 1. \quad (\text{A.4})$$

The intra-particle structure factor for a monodisperse cylinder (oblate or prolate) with radius  $R$  and length  $L$  is given by

$$P_{\text{cyl}}(Q) = \int_{\beta=0}^{\pi/2} \left[ \frac{2J_1(QR \sin \beta)}{QR \sin \beta} \frac{\sin((QL \cos \beta)/2)}{(QL \cos \beta)/2} \right]^2 \times \sin \beta d\beta, \quad (\text{A.5})$$

where  $J_1(x)$  represents a first-order Bessel function of the first kind and  $\beta$  is the orientational averaging angle. The monodisperse cylinder intra-particle structure factor may be separated into contributions from the radius ( $P_R$ ) and length ( $P_L$ ) terms as given by

$$P_{\text{cyl}}(Q, R, L) = P_R(Q, R) P_L(Q, L). \quad (\text{A.6})$$

In the limit when  $R \gg L$ , Pedersen [48] showed that the length contribution to the orientation integral in Eq. (A.5) was only significant when  $\cos \beta = 1$ . After subsequent substitution, the orientation integral only involves the particle radius. The intra-particle structure factor for an infinitely thin disk introduced by Kratky and Porod [52] is given by

$$P_R(Q, R) = \frac{2}{(QR)^2} \left[ 1 - \frac{J_1(2QR)}{QR} \right]. \quad (\text{A.7})$$

Substitution of Eq. (A.7) in Eqs. (A.5) and (A.6) removes the contribution of the particle radius to the orientation integral. Therefore, the orientation integral is no longer dependent on either the particle radius or length and the intra-particle structure factor for a monodisperse flat disk (i.e., oblate cylinder) may be written as [48]

$$P_{\text{ob},1}(Q) = 2 \left[ \frac{\sin(QL/2)}{QL/2} \right]^2 \left[ \frac{1 - J_1(2QR)/QR}{(QR)^2} \right]. \quad (\text{A.8})$$

Alternatively, the high  $Q$  region of a monodisperse flat disk may also be described by an exponential approximation [42] given by

$$P_{\text{ob},2}(Q) = \frac{2}{(QR)^2} \exp\left(-\frac{(QL)^2}{12}\right). \quad (\text{A.9})$$

Caution should be used when applying Eq. (A.9), as it does not exhibit plateau behavior in the low  $Q$  limit. For the ratio of  $R/L$  size parameter values observed in this study, Eq. (A.9) converges with Eq. (A.8) in the limited  $Q$  range roughly defined by  $QR > 3$ .

Because the radial dependence of the oblate cylinder form factor in Eq. (A.8) contains the Bessel function term, the combination of Eqs. (A.2) and (A.8) requires numerical techniques to solve the ensemble average integral. However, the  $J_1(x)$  Bessel function may be expanded in a polynomial

series given by

$$J_1(x) = \sum_{n=0}^{\infty} \frac{(-1)^n \left(\frac{1}{2}x\right)^{2n+1}}{n! \Gamma(n+2)}. \quad (\text{A.10})$$

Substitution of a 66-term polynomial series from Eq. (A.10) into Eq. (A.8) allows for a direct analytical solution to the ensemble average integral in Eq. (A.2) using the relation

$$\int_0^{\infty} x^n \exp(-ax) dx = \frac{\Gamma(n+1)}{a^{n+1}}. \quad (\text{A.11})$$

Because the 66-term polynomial expansion does not converge properly at higher  $Q$  values, the intra-particle structure factor in Eq. (A.8) is used for the polydisperse fits in the range  $QR < 3$ . In order to model the polydisperse radius oblate cylinders in the range  $QR > 3$ , the exponential approximation of the flat disk intra-particle structure factor is used in Eq. (A.2). Since the radius dependence in Eq. (A.9) is a polynomial, the ensemble average integral of the particle radius may be solved analytically using Eq. (A.11). The intra-particle structure factor used in this study to model polydisperse radius oblate cylinders thus takes the form

$$\langle P(Q) \rangle = \begin{cases} \frac{\int_0^{\infty} V^2 P_{\text{ob},1}(Q,R) f_s(R) dR}{\int_0^{\infty} V^2 f(R) dR}, & QR < 3, \\ \frac{\int_0^{\infty} V^2 P_{\text{ob},2}(Q,R) f_s(R) dR}{\int_0^{\infty} V^2 f(R) dR}, & QR > 3. \end{cases} \quad (\text{A.12})$$

The radius of gyration for a monodisperse circular cylinder is obtained from the length and radius parameters as given by

$$R_G^2 = \frac{L^2}{12} + \frac{R^2}{2}. \quad (\text{A.13})$$

The radius of gyration for a system of polydisperse radius cylinders is related to the sixth moment of the radius distribution given by [32]

$$\langle R_G \rangle^2 = \frac{L^2}{3} + \frac{\langle R^6 \rangle}{2 \langle R^4 \rangle}. \quad (\text{A.14})$$

## References

- [1] O.P. Strausz, P. Peng, J. Murgich, *Energy Fuels* 16 (2002) 809.
- [2] J.M. Sheremata, M.R. Gray, H.D. Dettman, W.C. McCaffrey, *Energy Fuels* 18 (2004) 1377.
- [3] M.R. Gray, *Energy Fuels* 17 (2003) 1566.
- [4] U. Bergmann, H. Groenzin, O.C. Mullins, P. Glatzel, J. Fetzer, S.P. Cramer, *Pet. Sci. Technol.* 22 (2004) 863.
- [5] H. Groenzin, O.C. Mullins, S. Eser, J. Mathews, M.G. Yang, D. Jones, *Energy Fuels* 17 (2003) 498.
- [6] M.M. Boduszynski, *Prepr. ACS Div. Pet. Chem.* 30 (1985) 626.
- [7] M.M. Boduszynski, *Energy Fuels* 2 (1988) 597.
- [8] P.M. Spiecker, K.L. Gawrys, P.K. Kilpatrick, *J. Colloid Interface Sci.* 267 (2003) 178.
- [9] J. Murgich, *Pet. Sci. Technol.* 20 (2002) 983.
- [10] N. Aske, H. Kallevik, E.E. Johnsen, J. Sjoblom, *Energy Fuels* 16 (2002) 1287.
- [11] I.H. Auflem, T.E. Havre, J. Sjoblom, *Colloid Polym. Sci.* 280 (2002) 695.
- [12] J.A. Ostlund, S.I. Andersson, M. Nyden, *Fuel* 80 (2001) 1529.
- [13] J.A. Ostlund, J.E. Lofroth, K. Holmberg, M. Nyden, *J. Colloid Interface Sci.* 253 (2002) 150.
- [14] C. Bardou, L. Barre, D. Espinat, V. Guille, M.H. Li, J. Lambard, J.C. Ravey, E. Rosenberg, T. Zemb, *Fuel Sci. Technol. Int.* 14 (1996) 203.
- [15] H.W. Yarranton, H. Alboudwarej, R. Jakher, *Ind. Eng. Chem. Res.* 39 (2000) 2916.
- [16] D. Fenistein, L. Barre, D. Broseta, D. Espinat, A. Livet, J.N. Roux, M. Scarsella, *Langmuir* 14 (1998) 1013.
- [17] C. Giavarini, D. Mastrofini, M. Scarsella, L. Barre, D. Espinat, *Energy Fuels* 14 (2000) 495.
- [18] Y. Bouhadda, D. Bendedouch, E. Sheu, A. Krallafa, *Energy Fuels* 14 (2000) 845.
- [19] W. Takeshige, *J. Colloid Interface Sci.* 234 (2001) 261.
- [20] P. Herzog, D. Tchoubar, D. Espinat, *Fuel* 67 (1988) 245.
- [21] D. Espinat, J.C. Ravey, V. Guille, J. Lambard, T. Zemb, *J.P. Cotton, J. Phys. IV* 3 (1993) 181.
- [22] Y.N. Xu, Y. Koga, O.P. Strausz, *Fuel* 74 (1995) 960.
- [23] L. Barre, D. Espinat, E. Rosenberg, M. Scarsella, *Rev. Inst. Fr. Pet.* 52 (1997) 161.
- [24] D. Fenistein, L. Barre, *Fuel* 80 (2001) 283.
- [25] T.G. Savvidis, D. Fenistein, L. Barre, E. Behar, *AIChE J.* 47 (2001) 206.
- [26] J.C. Ravey, G. Ducouret, D. Espinat, *Fuel* 67 (1988) 1560.
- [27] R.E. Overfield, E.Y. Sheu, S.K. Sinha, K.S. Liang, *Fuel Sci. Technol. Int.* 7 (1989) 611.
- [28] J.C. Ravey, D. Espinat, *Prog. Colloid Polym. Sci.* 81 (1990) 127.
- [29] E.Y. Sheu, K.S. Liang, S.K. Sinha, R.E. Overfield, *J. Colloid Interface Sci.* 153 (1992) 399.
- [30] Y.C. Liu, E.Y. Sheu, S.H. Chen, D.A. Storm, *Fuel* 74 (1995) 1352.
- [31] P. Thiyagarajan, J.E. Hunt, R.E. Winans, K.B. Anderson, J.T. Miller, *Energy Fuels* 9 (1995) 829.
- [32] M.Y. Lin, E.B. Sirota, H. Gang, *Abstracts Am. Chem. Soc.* 213 (1997) 66.
- [33] M. Sahimi, H. Rassamdana, *Physica A* 240 (1997) 419.
- [34] J.N. Roux, D. Broseta, B. Deme, *Langmuir* 17 (2001) 5085.
- [35] P.M. Spiecker, K.L. Gawrys, C.B. Trail, P.K. Kilpatrick, *Colloids Surf. A* 220 (2003) 9.
- [36] R. Tanaka, J.E. Hunt, R.E. Winans, P. Thiyagarajan, S. Sato, T. Takanohashi, *Energy Fuels* 17 (2003) 127.
- [37] A. Cosultchi, P. Bosch, V.H. Lara, *Colloid Polym. Sci.* 281 (2003) 325.
- [38] T.G. Mason, M.Y. Lin, *Phys. Rev. E* 67 (2003) 050401(R).
- [39] T.G. Mason, M.Y. Lin, *J. Chem. Phys.* 119 (2003) 565.
- [40] K.L. Gawrys, P.K. Kilpatrick, submitted for publication.
- [41] K.L. Gawrys, G.A. Blankenship, P.K. Kilpatrick, submitted for publication.
- [42] A. Guinier, G. Fournet, *Small Angle Scattering of X-Rays*, Wiley, New York, 1955.
- [43] X.J. Hu, K. Littrel, S. Ji, D.G. Pickles, W.M. Risen, *J. Non-Cryst. Solids* 288 (2001) 184.
- [44] S.H. Chen, J. Teixeira, *Phys. Rev. Lett.* 57 (1986) 2583.
- [45] J.S. Pedersen, *Adv. Colloid Interface Sci.* 70 (1997) 171.
- [46] M. Kotlarchyk, S.H. Chen, *J. Chem. Phys.* 79 (1983) 2461.
- [47] E.Y. Sheu, *Phys. Rev. A* 45 (1992) 2428.
- [48] J.S. Pedersen, *J. Appl. Crystallogr.* 33 (2000) 637.
- [49] H. Rassamdana, M. Sahimi, *AIChE J.* 42 (1996) 3318.
- [50] S. Acevedo, G. Escobar, M.A. Ranaudo, L.B. Gutierrez, *Fuel* 73 (1994) 1807.
- [51] M.N. Siddiqui, M.F. Ali, J. Shirokoff, *Fuel* 81 (2002) 51.
- [52] O. Kratky, G. Porod, *J. Colloid Sci.* 4 (1949) 35.